


RESEARCH ARTICLE

A patterned mechanical–electrical coupled sensing patch for multimodal muscle function evaluation

Jiangtao Xue^{1,2} | Yang Zou^{1,2} | Zhirong Wan³ | Minghao Liu² |
 Yiqian Wang^{2,4} | Huaqing Chu^{2,5} | Puchuan Tan^{2,6} | Li Wu² |
 Engui Wang² | Han Ouyang⁶ | Yulin Deng¹ | Zhou Li^{2,3,6} 

¹School of Medical Technology, Beijing Institute of Technology, Beijing, the People's Republic of China

²Beijing Institute of Nanoenergy and Nanosystems, Chinese Academy of Sciences, Beijing, the People's Republic of China

³Department of Neurology, Aerospace Center Hospital, Beijing, the People's Republic of China

⁴Center on Nanoenergy Research, School of Physical Science and Technology, Guangxi University, Nanning, the People's Republic of China

⁵Department of Anesthesiology National Cancer Center, National Clinical Research Center for Cancer, Cancer Hospital Chinese Academy of Medical Sciences, Peking Union Medical College, Beijing, the People's Republic of China

⁶School of Nanoscience and Engineering, University of Chinese Academy of Sciences, Beijing, the People's Republic of China

Correspondence

Yang Zou and Yulin Deng, School of Medical Technology, Beijing Institute of Technology, Beijing 100081, the People's Republic of China.

Email: zouyang@bit.edu.cn and deng@bit.edu.cn

Zhou Li, Beijing Institute of Nanoenergy and Nanosystems, Chinese Academy of Sciences, Beijing 101400, the People's Republic of China.

Email: zli@binn.cas.cn

Funding information

National Key Research and Development Program of China, Grant/Award Number: 2022YFE0111700; National Natural Science Foundation of China, Grant/Award Numbers: T2125003, 82202075; Beijing Natural Science Foundation, Grant/Award Number: L212010; National Postdoctoral Program for Innovative Talents, Grant/Award Number: BX20220380; China Postdoctoral Science Foundation, Grant/Award Number: 2022M710389; Fundamental Research Funds for the Central Universities

Abstract

Muscles, the fundamental components supporting all human movement, exhibit various signals upon contraction, including mechanical signals indicating tremors or mechanical deformation and electrical signals responsive to muscle fiber activation. For noninvasive wearable devices, these signals can be measured using surface electromyography (sEMG) and force myography (FMG) techniques, respectively. However, relying on a single source of information is insufficient for a comprehensive evaluation of muscle condition. In order to accurately and effectively evaluate the various states of muscles, it is necessary to integrate sEMG and FMG in a spatiotemporally synchronized manner. This study presents a flexible sensor for multimodal muscle state monitoring, integrating serpentine-structured sEMG electrodes with fingerprint-like FMG sensors into a patch approximately 250 μm thick. This design achieves a multimodal assessment of muscle conditions while maintaining a compact form factor. A thermo-responsive adhesive hydrogel is incorporated to enhance skin adhesion, improving the signal-to-noise ratio of the sEMG signals (33.07 dB) and ensuring the stability of the FMG sensor during mechanical deformation and tremors. The patterned coupled sensing patch demonstrates its utility in tracking muscular strength, assessing fatigue levels, and discerning features of muscle dysfunction by analyzing the time-domain and frequency-domain characteristics of the mechanical–electrical coupled

This is an open access article under the terms of the [Creative Commons Attribution](https://creativecommons.org/licenses/by/4.0/) License, which permits use, distribution and reproduction in any medium, provided the original work is properly cited.

© 2024 The Author(s). *InfoMat* published by UESTC and John Wiley & Sons Australia, Ltd.

signals, highlighting its potential application in sports training and rehabilitation monitoring.

KEYWORDS

mechanical–electrical coupled, multimodal sensing, muscle function evaluation

1 | INTRODUCTION

The muscular system is vital for human biomechanics, supporting daily activities and tasks.¹ Assessing its state is essential for athletic performance, health, sports science, rehabilitation, and chronic disease management. Muscle contraction, driven by neural action potentials, generates both electrical and mechanical signals. These signals offer unique insights into muscle activity and condition, aiding in a comprehensive understanding of muscle functionality. Electrical signals, in particular, reveal changes in electric potential during muscle stimulation, providing valuable information on muscle strength, activation levels, and motor control.^{2,3} Mechanical signals reflect changes in characteristics like deformation and vibration during muscle contraction. They indicate the speed of contraction, level of fatigue, and distribution of muscle fiber types.^{4–6} With the ongoing advancement of sensing technology,^{7,8} noninvasive methods for monitoring muscle conditions have emerged as a significant area of interest in both research and practical applications.^{9–13} Real-time monitoring of multimodal muscle activity maximizes athletic performance, evaluates patient progress in rehabilitation, and enhances fitness training regimens.^{14–18}

Surface electromyography (sEMG) uses electrodes on the skin to capture real-time, dynamic muscle electrical signals. It evaluates muscle activation, fatigue, and coordination by analyzing signal intensity and patterns.¹⁹ The root mean square (RMS) value of sEMG evaluates muscle strength by reflecting voltage variations, indicating neural excitation and muscle strength.^{20–22} In designing wearable electrodes, reducing skin-electrode interface impedance is crucial for acquiring high-quality sEMG signals.²³ Force myography (FMG) is a noninvasive method that detects mechanical changes in muscles by measuring stiffness variations in the Muscle-Tendon Complex (MTC) during activation. This is usually done by placing a force sensor on the target area and applying a pre-tension force.^{24,25} The standard deviation (SD) of FMG signals, which reflect tremors during muscle contractions, can indicate muscle fatigue by evaluating the consistency and coordination of muscle activity.^{26–28} FMG utilizes force sensors on the skin to quantitatively assess muscle contraction force. Various sensor types include

piezoresistive,²⁹ capacitive,³⁰ piezoelectric,³¹ photoelectric,³² and so on. Piezoelectric and piezoresistive sensors, known for their dynamic response sensitivity and rapid response characteristics, are widely used in FMG to gather mechanical information on muscle contractions.^{25,29} Due to their size and simplified power management, piezoelectric sensors are chosen as the core component for FMG. They effectively respond to time-frequency characteristics during continuous muscle contractions and, when combined with sEMG electrode data, provide a comprehensive assessment of muscle state.

sEMG and FMG monitor different signal types during muscle contractions, reflecting distinct characteristics of muscle status.^{33–35} A single information source is insufficient to comprehensively assess muscle status. Hence, it is necessary to combine the two methods for a comprehensive assessment of muscle status.^{36–38} In designing wearable sensors for multimodal monitoring, key factors include stretchability, flexibility, and comfort to fit various muscles, ensuring strong skin adhesion for both sEMG and FMG. The sEMG signal quality depends on electrode-skin impedance, while FMG stability relies on preload force. Achieving spatiotemporal synchronization of mechanical–electrical signals is essential, enabling simultaneous collection during muscle contractions without adding bulk or complexity.^{39,40}

Currently, some researchers mostly combine mature or commercial sEMG and FMG sensor systems using straps to collect forearm and hand movement information. By leveraging artificial intelligence methods, they have achieved applications in human-machine interaction, such as gesture recognition and prosthetic control. The results indicate that the coupling of the two methods further enhances the efficiency and accuracy of AI algorithms. However, since most approaches use existing commercial sensors and modules, the resulting systems are relatively large and lack flexibility, limiting their usability in various scenarios. Moreover, although the coupling approach improves algorithmic recognition results, existing research still lacks an interpretation of the characteristics of the two types of signals.^{41–44} Here, we presented a novel design of a patterned mechanical–electrical coupled sensing patch (PCSP) for real-time testing of muscle status. PCSP is a sensor patch with a

thickness of approximately 250 μm , a weight of about 200 g, and a water vapor transmission rate of 51 g/($\text{m}^2 \text{ h}$). The patch consists of serpentine sEMG electrodes and a fingerprint-like force FMG sensor for measuring electrical and mechanical signals during muscle activity, respectively. The design of the serpentine structure enables the electrodes to conformally adhere to muscles in various states, thereby enhancing the signal stability of sEMG. The fingerprint-like structure, while ensuring stretchability, can provide an excellent output response to mechanical stimuli at different angles. The two sensors are laminated together with ultrathin PDMS films, conducting spatiotemporally synchronized tests on muscle status from both mechanical and electrical information perspectives. The simulation results and experimental validation findings indicate that the coupled patch remains stable when subjected to a strain of up to 30% and maintains its performance after over 15 000 stretch tests. In order to reduce the resistance between the patterned sEMG dry electrodes and the skin and to maintain the necessary preload force for the FMG sensor when the muscle undergoes mechanical deformation, a hydrogel adhesion layer is designed that enhances adhesion as the temperature increases. With the help of the adhesive layer, the sEMG signal exhibits a signal-to-noise ratio (SNR) of 33.07 dB, and the FMG sensor displays reliable and consistent performance. PCSP enables synchronous measurement of mechanical and electrical signals during muscle contraction, providing complementary information for evaluating muscle strength and fatigue. In ankle extension tests, PCSP monitored gastrocnemius and tibialis anterior muscles, revealing distinct time-frequency characteristics in Parkinson's patients compared to healthy individuals, demonstrating PCSP's potential in diagnosing muscle dysfunction.

2 | RESULTS AND DISCUSSION

2.1 | Overview of patterned mechanical–electrical coupled sensor patch

The patterned mechanical–electrical coupled sensor patch (PCSP) is presented in Figure 1A. The PCSP is primarily composed of four components stacked from top to bottom: the sEMG electrodes layer, the substrate layer, the FMG sensor, and the adhesive layer. Based on the principle of spring, the sEMG electrodes are designed with a centrally symmetric, serpentine, and meandering structure to ensure stretchability. The patterned sEMG electrodes consist of a two-layer structure, with the top layer in direct contact with the skin being gold-coated (approximately 100 nm) for high conductivity,

biocompatibility, and oxidation resistance. The bottom layer, a polyimide (PI) film (50 μm), functions as an elastic support for structural resilience. The substrate layer comprises two ultra-thin, transparent, and stretchable polydimethylsiloxane (PDMS) layers, each 40 μm thick, serving as the substrate for sEMG electrodes and FMG sensor, respectively, and effectively integrating both components. The FMG sensor utilizes a fingerprint-like silver-plated polyvinylidene difluoride (PVDF) film (52 μm), encapsulated by polytetrafluoroethylene (PTFE) films (8 μm) on both top and bottom to enhance the resilience, resulting in a planar omnidirectionally stretchable piezoelectric FMG sensor for the sensitive detection of multi-directional mechanical force signals. A thermo-responsive hydrogel composed of polyvinyl alcohol (PVA), branched polyethyleneimine (b-PEI), and CaCl_2 is employed as an adhesive layer (approximately 100 μm) in conjunction with the patterned mechanical–electrical coupled sensors. Upon exposure to human body temperature, the adhesive hydrogel facilitates a secure and intimate attachment of the patterned coupled sensors to the skin, reducing the contact impedance between the sEMG electrodes and the skin, while providing the necessary pretensioning force for the FMG sensor during stretching activities.

Muscular contractions in diverse body areas may lead to deformations of varying directions. The favorable flexibility, thinness, and stretchability of the PCSP allow for conformal matching with muscles in various parts of the human body and adapt to deformations of differing degrees of stretch. The photo of integrated PCSP, as shown in Figure 1B, has an overall thickness of approximately 250 μm without the adhesive layer. It is worth mentioning that the 250 μm thick PCSP also has a good water vapor transmission rate, which would reduce discomfort caused by sweating (Figure S1). With the help of the adhesive hydrogel, the PCSP can be affixed to the skin conformally. Figure 1C displays the physical photographs and simulation results of the PCSP in its initial, stretched, bent, and twisted states, demonstrating the ability to withstand varying force situations for viability in various testing scenarios. Figure 1D shows a schematic flowchart illustrating the use of PCSP for the analysis of multimodal muscle states. When the subject performs intentional movements (such as rapid foot tapping or finger tapping), the muscles exhibit two different types of signals, including mechanical signals like muscle deformation or tremors, as well as myoelectric signals. These signals can be simultaneously captured by the two types of sensors in the coupled sensing patch. The serpentine sEMG electrodes are used to detect myoelectric signals, while the fingerprint-like FMG sensors are used to detect mechanical signals. These two signals are transmitted to

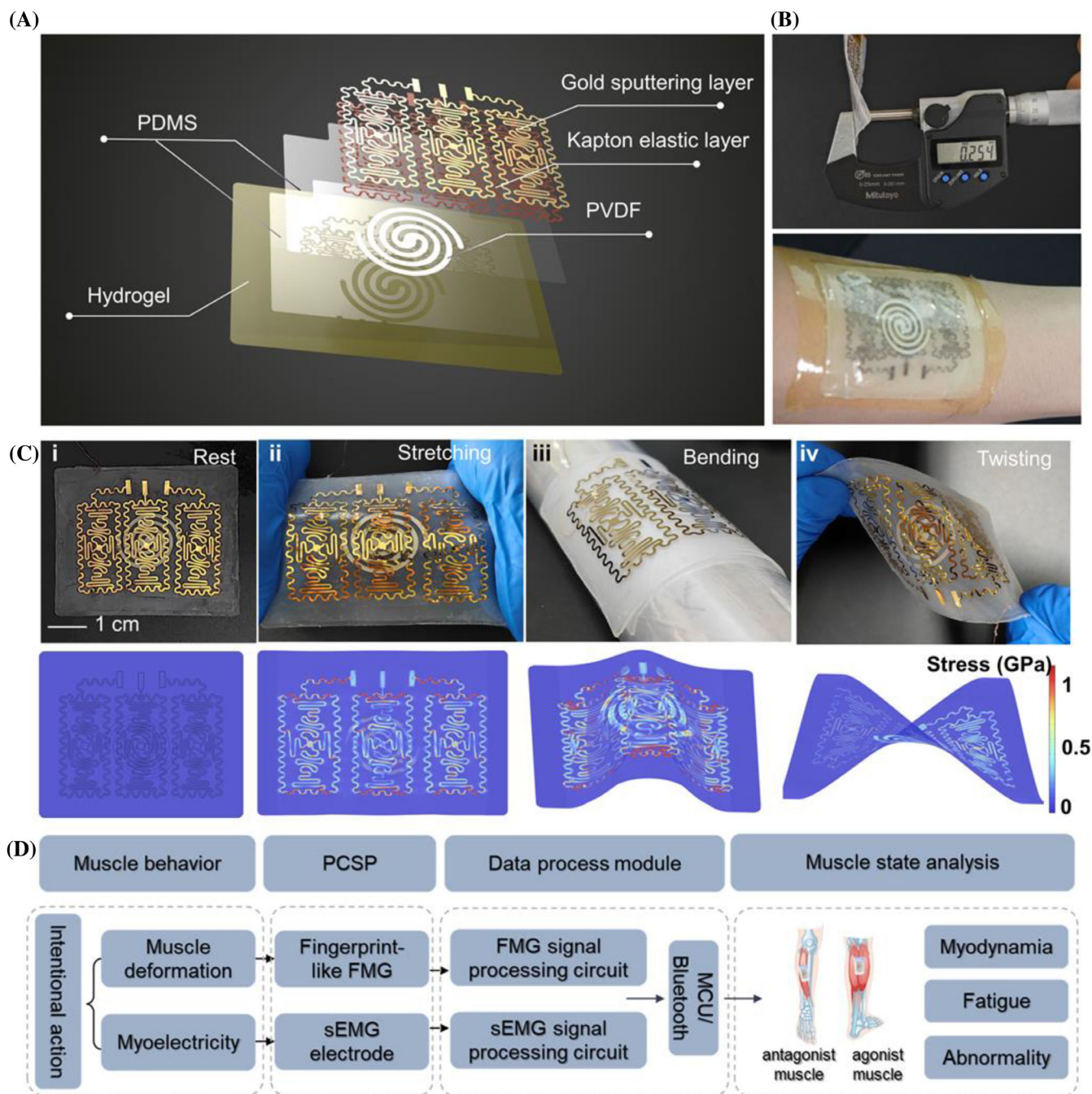


FIGURE 1 Overview and design of PCSP. (A) Explosion diagram of PCSP. (B) Display of photos of PCSP thickness measurement and attachment on skin. (C) Physical photos and finite element analysis results of PCSP in four different states: Rest, stretching, bending, and twisting. (D) Flowchart of PCSP used for the process from muscle behavior monitoring to muscle state analysis.

the computer terminal through the signal acquisition circuit board shown in Figure S2 (power supply module, FMG signal processing module, sEMG signal processing module, and Bluetooth module). The detailed circuit schematic is shown in Figure S3. Then, the time-domain and frequency-domain characteristics of the two signals are extracted and analyzed, which are finally used for the evaluation of muscle strength, fatigue level, and muscle function abnormalities.

2.2 | Characterization of mechanical properties and mechanical response of PCSP

The design of flexible electronics should be tailored to match the modulus of muscle and skin tissues, which can reduce stress concentration at the interface, maintain interface stability, and prevent displacement under mechanical deformation.⁴⁵ The stretchability and

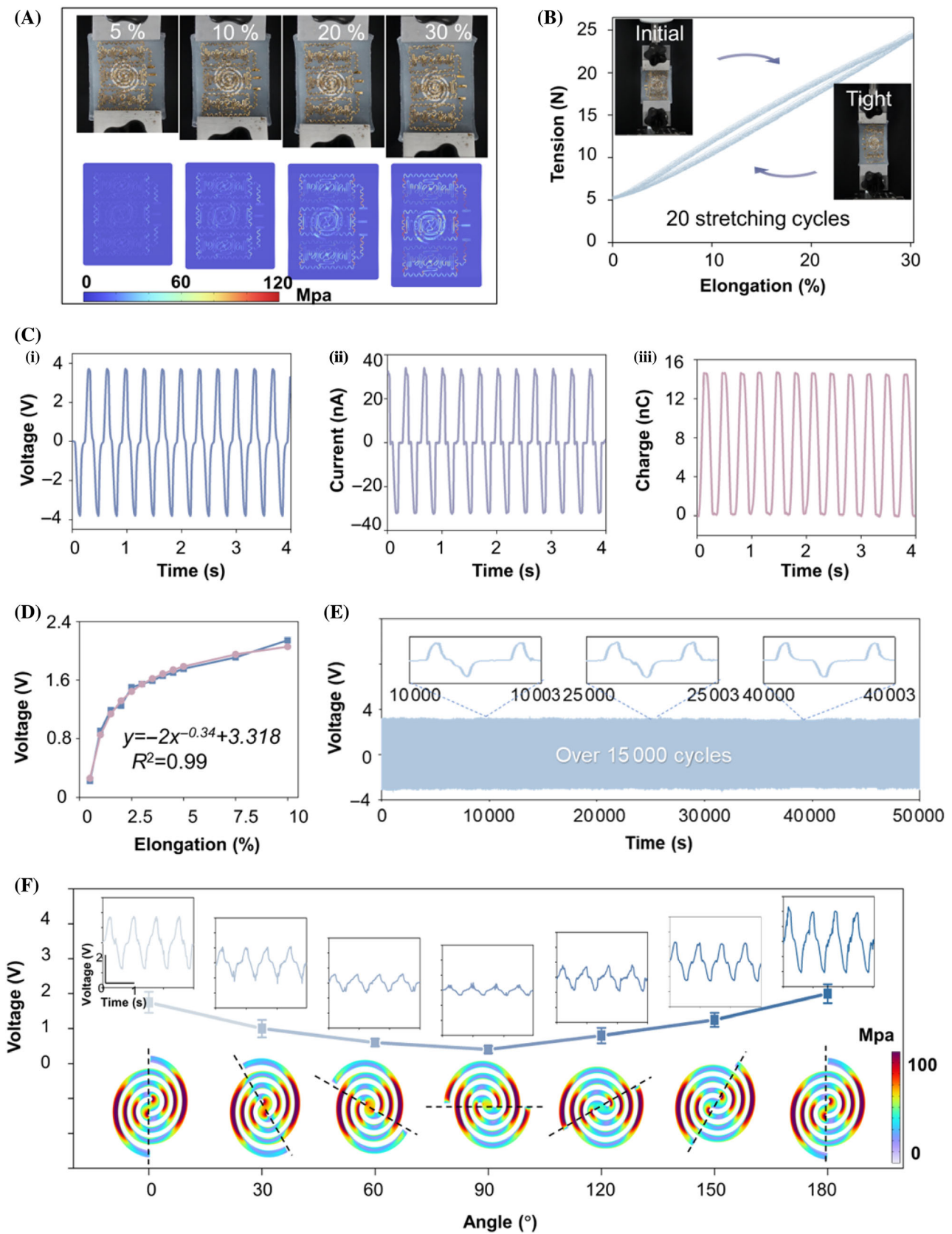


FIGURE 2 Legend on next page.

modulus of PCSP have been evaluated through theoretical finite element analysis and stretch testing. Using finite element analysis software, the stretchability of the basic electrode structure was simulated (Figure S4), with stretches of 25% longitudinally and 20% transversely. The simulations showed no significant stress concentration at the meandering junctions and an even distribution of stress within the serpentine structures, confirming the designed pattern's stretchability and structural stability. Figure 2A demonstrates the verification of the device's stretching performance using a digital force gauge (Mark-10). The calculation formula for strain is: $\varepsilon = \Delta l / l_0$, where ε represents the magnitude of strain, Δl represents the displacement of the upper clamp from its initial position, and l_0 represents the initial length of the device. Considering that the strain induced by muscle contractions is relatively minor, with muscle fiber lengths altering by approximately 10% during regular movements from a resting state. Here, tensile experiments were executed using four distinct levels of strain, varying from 5% to 30%, to assess the overall deformation and stability of the device under various conditions. The internal fingerprint-like FMG sensor and serpentine sEMG electrodes of PCSP successfully endured stretching ranging from 5% to 30% without any notable instability, confirming the robust stability of PCSP even under a 30% stretching strain. The stress distribution of PCSP at different elongations has been calculated via finite element analysis software COMSOL Multiphysics, further validating the structural stability of the PCSP.

The stretching lengths of PCSP were recorded during the stretching experiment, in order to estimate the Young's modulus of the device. The data presented in Figure 2B represents the force-displacement curves of PCSP subjected to 30% strain in 20 repeated tests. Assuming that PCSP acts as a linear elastic material, Young's modulus of the device may be estimated using the formula $E = \delta / \varepsilon$, where δ is the stress, approximated as $\delta = F / A$, F is the applied force, and A being the cross-sectional area of the PCSP. The calculation results in Young's modulus of approximately 4.5 MPa for the device, which is of a similar magnitude to that of skeletal muscle.⁴⁶ The inconsistency in the force-displacement curve during the loading and unloading of tensile force illustrated in the figure is due to the viscoelastic nature of PCSP. The viscoelasticity is particularly noticeable at

lower frequencies, which explains the observed hysteresis phenomena throughout the stretching and relaxing process. The hysteresis loop area of PCSP is calculated to be 23.04 J, which means the energy loss per cycle is approximately 23.04 J.

The mechanical response and electrical output performance of the FMG sensor were further evaluated during the stretching process. Figure 2C displays the electric output of the fingerprint-like FMG sensor when the PCSP was subjected to a 30% strain. The peak of open-circuit voltage was approximately 4 V, the peak of short-circuit current was around 30 nA, and the peak of the cyclic flow of charge was approximately 14 nC. The electrical output of the FMG sensor under different elongations was tested, with different elongations (0%–10%) set using a Mark-10 according to common elongation of muscle fibers, and the output voltage of the piezoelectric sensor under different conditions was collected using an oscilloscope. The elongation-electricity relationship of the fingerprint-like FMG sensor is shown in Figure 2D, and the collected data were imported into Origin for fitting, obtaining a comparison between the fitted curve (purple) and the actual curve (blue). The expression for the fitted curve is $y = -2x^{-0.34} + 3.318$, where y represents the voltage output, and x represents the magnitude of strain. The coefficient of determination (R^2) for the fitted curve is 0.99. The goal of the fitted curve is to derive the strain information of the FMG sensor from its electrical output, thereby obtaining the mechanical signal of muscle reaction. The results indicate that compared to large strains, electrical signals exhibit more pronounced changes with strain in the small strain range, suggesting that the sensor is more sensitive to small strains and has the potential for monitoring weak muscle movement signals. The endurance of the FMG sensor was also evaluated, as depicted in Figure 2E. Following over 15 000 stretching tests on the FMG sensor, it was observed that during a 50 000-s fatigue test, there was virtually no change in output. The rate of change in amplitude is approximately 0.00012 %/s, demonstrating the good stability of its sensing performance.

Subsequently, finite element analysis is performed to confirm that the fingerprint-like PVDF film not only possesses multidirectional stretchability but also demonstrates a good electrical response to deformations from different directions (Figure S5). Then, an experimental

FIGURE 2 Stretch test of PCSP. (A) Experimental photos by Mark-10 and simulation calculation results by COMSOL of stretching PCSP from 5% to 30%. (B) Force-displacement curves in 20 cycles of stretch tests from 0% to 30% strain measured with Mark-10. (C) Voltage, current, and transferred charge output of fingerprint-like FMG sensor stretched to 30% strain. (D) Electrical output curves, fitting curves, and corresponding formulas of FMG sensor under different strains. (E) Durability test of FMG sensor. (F) Voltage output of FMG sensor at 30% strain under different angles.

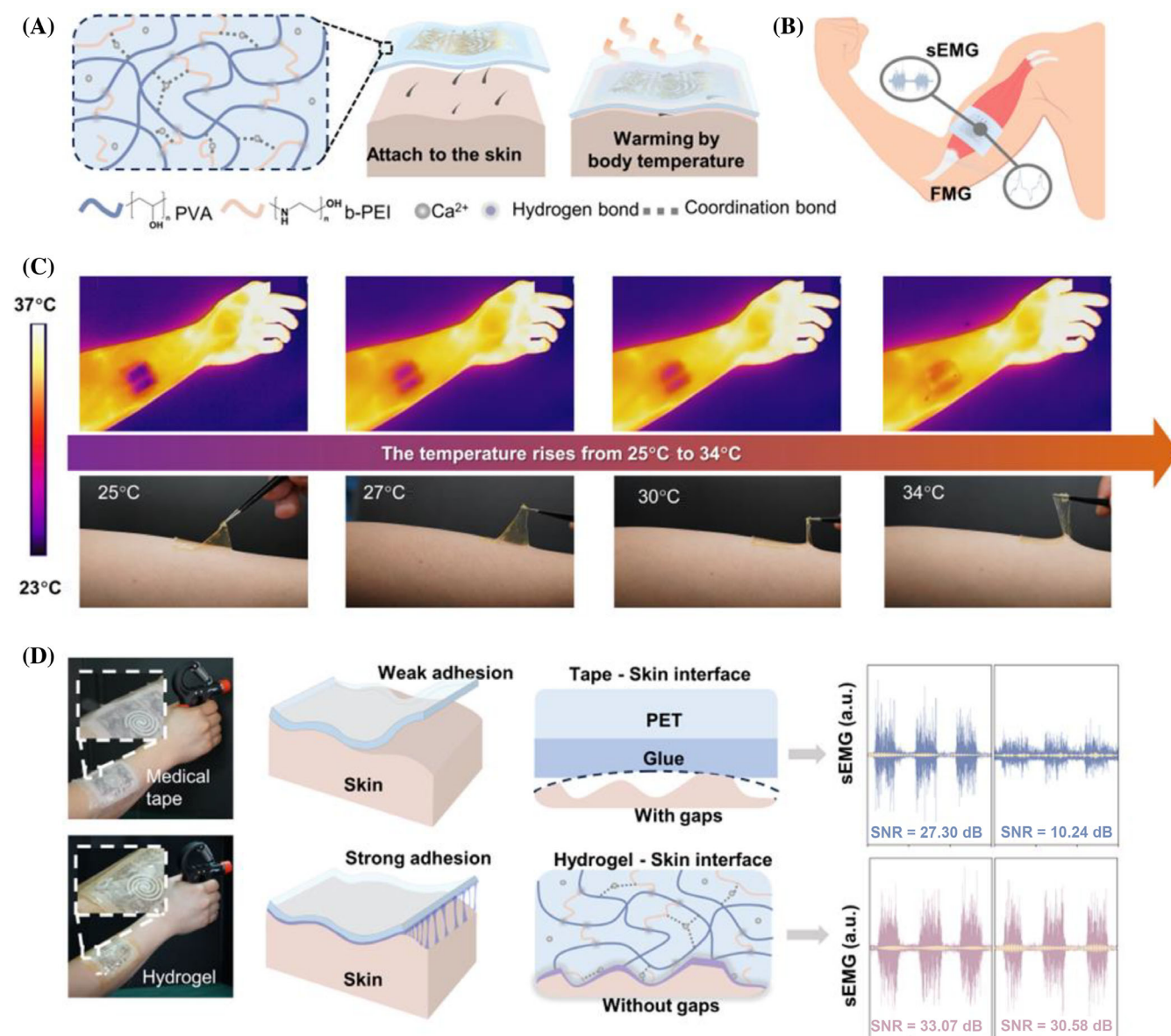


FIGURE 3 Composition and performance characterization of temperature-sensitive hydrogel adhesive layer. (A) Components of hydrogel, cross-linking network, and the principle of enhanced adhesion with temperature increase. (B) Schematic diagram of PCSP using hydrogel adhesive layer attached to the muscle epidermis. (C) Characterization of adhesion between hydrogel and skin during the process of increasing temperature from 25°C to 34°C. (D) Comparison of adhesion smoothness between hydrogel and medical tape as adhesive layers and the corresponding sEMG SNR.

validation was performed to confirm the output of sensors that had been deformed in various directions. This was achieved by stretching the PCSP at different angles, as illustrated in Figure 2F. In accordance with theoretical simulation calculations, the device exhibits a favorable electrical output response when subjected to stretching at various angles. The output voltage of the FMG sensor reaches its maximum value at an angle of 0° and decreases to the lowest value when rotated to 90°, then gradually increases as it continues to spin to 180°. This demonstrates the favorable responsiveness of PCSP to

mechanical stimuli in various directions, ensuring its suitability for effectively detecting mechanical signals from muscles with diverse contraction orientations.

Finally, we investigated the effect of stretching on sEMG signals. We used Mark-10 to stretch the PSCP and tested the change in electrode resistance as the PSCP elongation rate varied from 0% to 30% (Figure S6). From Figure S6, it can be seen that when the electrode's elongation rate is less than 10%, the change in electrode resistance is minimal. As the device is further stretched, the electrode resistance increases from 40 Ω to 60 Ω . This

demonstrates that the stretching of the PCSP within the range of muscle contraction does not significantly affect the quality of the sEMG signal.

2.3 | Thermo-responsive adhesive hydrogel for myoelectric signal enhancement

The performance of the sEMG electrode with a serpentine flexible construction was evaluated while measuring muscle contraction, as illustrated in Figure 3A. The device gathered myoelectric signals from the biceps while performing a bicep curl motion, which was compared to the signals obtained from commercially available gel-based Ag/AgCl electrodes. The medical polyethylene terephthalate (PET) tape was used to attach the PCSP to the skin. The results indicated that the signal quality of the dry electrode was virtually identical to that of the commercial electrode (as depicted in Figure S7).

In order to improve the signal quality in long-term monitoring, an adhesive layer made of hydrogel was developed to minimize the contact impedance between the PCSP and the skin. This adhesive layer's stickiness is enhanced as the temperature increases.⁴⁷ The inclusion of this sticky layer serves two purposes: enhancing the signal quality of the sEMG and providing the necessary preload force to maintain the stability of the FMG sensor during stretching or vibration. Here we utilized a thermally enhanced adhesive hydrogel that was constructed using a noncovalent crosslinked network, as depicted in Figure 3B. The hydrogel was constituted of PVA, b-PEI, and CaCl₂. The first network is formed by the hydrogen bonds between the —OH groups in PVA and the —NH₂ groups in b-PEI. When CaCl₂ is added, the —OH/—NH₂ groups form coordination bonds with Ca²⁺, resulting in the formation of a second network. The hydrogel possesses exceptional conformability due to its dynamic interactions, enabling it to adhere tightly to uneven surfaces. The rich polar groups —OH and —NH₂ within the hydrogel form reversible adhesion through hydrogen bonds and electrostatic interactions with the skin. Furthermore, the adhesiveness of the noncovalent dynamic network and the small molecules of b-PEI is enhanced when the temperature rises due to their temperature-responsive rheological properties, resulting in a seamless bond.^{48,49}

The thermo-responsive adhesive capability of the material was examined by measuring the viscosity of the hydrogel adhered to the skin at different temperatures, as shown in Figure 3C. Thawed hydrogel was applied to the skin, and the change in adhesive force with increasing temperature was observed. The figure clearly

demonstrates that the adhesive force between the hydrogel and the skin increases steadily as the temperature increases from 25°C to 34°C, and the hydrogel demonstrates strong adherence at body temperature. To further verify the effect of temperature on the adhesiveness of the hydrogel, the peel force of the hydrogel tightly adhered to the pigskin was tested using a Mark-10. A T-peel test was conducted (Figure S8), during which the peel force was measured as the displacement increased until a steady state was reached. The force at this steady state is referred to as F_{peel} , and the interface toughness is calculated as twice the ratio of F_{peel} to the sample width.^{47,50,51} As shown in the figure, the interface toughness is observed to increase with rising temperature, with a rapid increase occurring near body temperature, demonstrating the characteristic of enhanced adhesiveness of the hydrogel with temperature. When comparing the proposed adhesive hydrogel with the medical tape in long-term monitoring, the hydrogel demonstrates an advantage in terms of close contact with the skin, as depicted in Figure 3D. After attaching the PCSP to the same location using both the hydrogel and medical tape, and performing 60 rapid clench-and-release actions, it was observed that, compared to medical tape, the hydrogel demonstrated a superior conformal ability to the skin during continuous movements. The presence of hair and wrinkles on the skin makes it difficult for ordinary medical tape to fully conform and adhere to the skin. However, using the adhesive hydrogel under body temperature conditions, based on the thermo-responsive rheological properties of the noncovalent dynamic network and b-PEI small molecules, its adhesion strength is enhanced, forming a gapless contact with the skin. With the help of the thermo-responsive hydrogel adhesive layer, the SNR of the PCSP's electromyographic signals remained almost unchanged, maintaining at 30.58 dB after 60 repeated cycles of muscle contraction and relaxation. In contrast, the SNR of the PCSP adhered with medical tape rapidly decreased from 27.3 to 10.24 dB after 60 repeated cycles.

The impact of using adhesive hydrogel on the stability of FMG sensors has also been verified. Three control groups were set up: one using medical tape, another using adhesive hydrogel, and the third using common straps. We tested the changes in FMG signals during continuous muscle contractions under these three different attachment methods (Figure S9). By comparing the FMG signal changes, we found that using medical tape caused distortion and offset in the FMG signals during continuous contractions. In contrast, adhesive hydrogel and straps maintained FMG signal stability, proving that adhesive hydrogel can meet the pretensioning needs of FMG sensors during deformation and rebound processes.

Finally, we tested the impact of temperature and humidity changes on the output performance of the coupled sensing system after applying the hydrogel adhesive layer. The test results indicate that changes in temperature and humidity do not significantly affect the output of both sEMG and FMG sensors (Figures S10 and S11).

2.4 | Application in the assessment of muscle strength and fatigue

After characterizing the performance of the PCSP, its application in assessing muscle strength and fatigue status was further demonstrated. In this study, muscle strength and fatigue characteristics were evaluated in a group of young healthy males. Four subjects, aged 20–30 years, with heights of 170–180 cm and weights of 60–80 kg, were selected. Similar data characteristics were exhibited during the tests, and therefore, a single set of data from this group was chosen for display. The PCSP

was utilized to evaluate muscle condition across various intensities of strength exercise. The assessment involved conducting a grip strength test at five different levels of strength, ranging from 5 to 40 kg (Figure 4A). During the experiment, participants wearing the PCSP executed a grip and release action five times at each training level, while the electrical and mechanical signals of the forearm extensor muscles were monitored synchronously. The next level of strength grip testing proceeded after a sufficient period of rest. A metronome was employed to maintain the uniformity of timing for each action, resulting in a nearly equivalent speed of the grip motion across different levels of strength. As illustrated in Figure 4B, the output signal from the FMG sensor is indicated by the blue line, while the sEMG signal is depicted by the purple line. The output of the FMG sensor exhibits an initial increase followed by stabilization as the strength is increased. The occurrence of this pattern is due to the FMG sensor's ability to monitor the deformation and mechanical vibration resulting from muscular

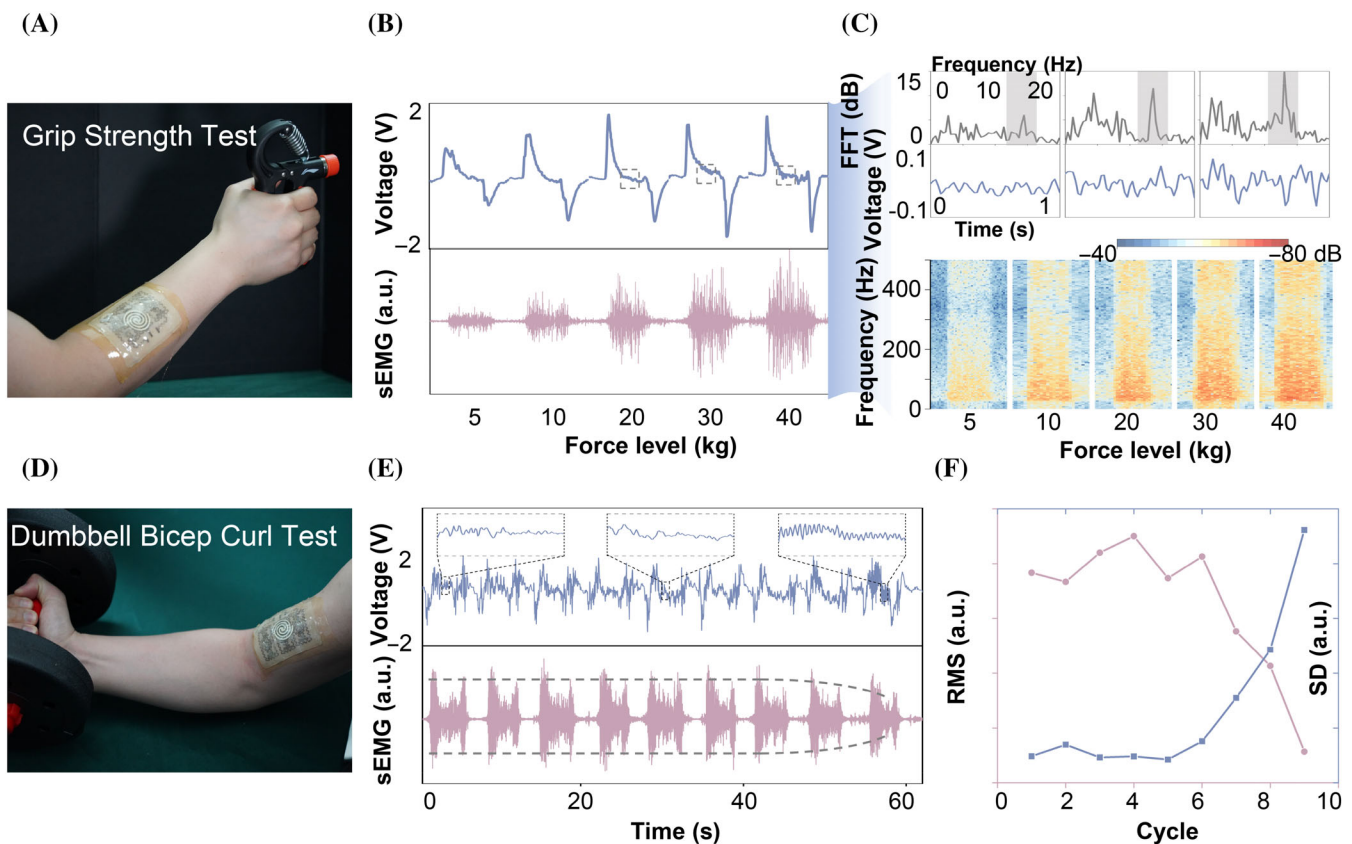


FIGURE 4 Application demonstration of PCSP in muscle strength and muscle fatigue level assessment. (A) Photo of PCSP attached to the forearm for grip strength testing. (B) Voltage output of FMG (top) and output of sEMG electrodes (bottom) at different grip strengths. (C) Amplified waveform of FMG voltage output and amplitude-frequency curve after FFT for 20–40 kg grip strength (top), and time-frequency graph of sEMG signal after STFT (bottom). (D) Photo of PCSP attached to the epidermis of the biceps for curl testing. (E) Voltage output of FMG corresponding to the last nine sets in fatigue Testing (top) and output of sEMG electrodes (bottom). (F) Changes in the RMS of electromyography signals and the SD of FMG sensors during fatigue testing.

activity, namely the contraction of muscle fibers. The mechanical signal response changes depending on the intensity of muscle contraction. At lower to moderate levels of strength, the magnitude of the mechanical signal rises as strength increases. However, as the level continues to rise, the pace at which the magnitude grows gradually decreases. Maximum voluntary contraction (MVC) is a crucial measure of muscular strength that is commonly employed to evaluate muscle function, the effects of illnesses, or the advancement of rehabilitation. When a muscle reaches or approaches its MVC, its ability to deform is restricted by its structural and physiological properties. This can result in a plateau or even a decline in the pace and extent of muscle fiber deformation. Furthermore, it is evident that when strength increases, the amplitude of the electromyographic signal consistently increases. The increase is a result of the recruitment of additional muscle fibers involved in the contraction as strength improves, resulting in a rise in the amplitude of the electromyographic signal. This signal reflects the level of electrical activity occurring within the muscle.

At increasing levels of muscular strength, the mechanical signals convey different features compared to the electrical signals of muscle activity. As indicated in the upper graph of Figure 4C, there is an enlarged view of the output waveform from the FMG sensor ranging from 20 to 40 kg, as well as a frequency domain diagram resulting from a Fast Fourier Transform (FFT) of Figure 4B. The boxed area in Figure 4B corresponds to the continuous exertion phase during the grip strength test. A discernible tremor can be noticed in the muscles when subjected to a sustained force that exceeds 20 kilos in grip strength testing. This is because at the limits of muscle strength, muscle fibers typically exhibit intermittent contractions or asynchrony in contractions among fibers. By examining the magnified waveform in Figure 4C, it can be found that when training is conducted at higher force levels, the amplitude of the muscle tremor signals increases as the strength increases. Similarly, the graph in the frequency domain after performing the FFT shows that when the intensity increases, the amplitude of the tremor signals at roughly 15 Hz also increases. This suggests that the tremor signals occupy a bigger share of the overall signal. Therefore, characteristics such as the amplitude and frequency of the mechanical signals monitored by the FMG sensor have significant implications for the assessment of muscle strength. The bottom section of Figure 4C shows a time-frequency plot generated by applying a Short-time Fourier transform (STFT) to the sEMG waveform from Figure 4B. The plot demonstrates a direct correlation between muscle strength and the constant increase in sEMG frequency. This phenomenon occurs because

slow-twitch fibers are recruited initially as strength levels start to rise. As the force increases, bigger and quicker fast-twitch muscle fibers are also activated, leading to the production of high-frequency signals. In addition, as the need for strength increases, the motor neurons discharge more often, resulting in a rise in the high-frequency components of the myoelectric signal.

Subsequently, the feasibility of using PCSP for muscle fatigue assessment was further investigated. The evaluation specifically examined the alterations in electrical and mechanical signals of the biceps brachii while performing a continuous bicep curl dumbbell test, as illustrated in Figure 4D. The testing procedure required the participant to wear the PCSP as shown, and to repetitively perform bicep curls with a 30 kg dumbbell to the rhythm set by a metronome, continuing until significant muscle fatigue behavior emerged, prompting cessation. The latest nine sets of data from the testing process were chosen for further analysis, as shown in Figure 4E. Similarly, the blue curve corresponds to the signal obtained from the FMG sensor, and the purple curve corresponds to the sEMG signal. During the gradual muscle fatigue process, there was no significant drop in the amplitude of the FMG signal. However, the feature of muscular tremors in mechanical signals became more noticeable as the prolonged exercise continued, indicating the appearance of muscle fatigue, especially in the last two cycles. As the degree of muscular tiredness escalated, the sEMG signal demonstrated a notable decrease in amplitude. Figure 4F displays the time-domain features of the electrical and mechanical signals calculated from the raw data, which include the root mean square (RMS) of the sEMG signal and the standard deviation (SD) of the mechanical signal. RMS is a frequently employed time-domain characteristic in the processing of sEMG signals to measure the intensity of muscle activity, which is valuable for assessing muscle exhaustion. It can be calculated by

$$MS = \sqrt{\frac{1}{k} \sum_{i=1}^k y_i^2}, \text{ where } k \text{ represents the number of data}$$

points in the selected data segment, and y_i corresponds to the value of the sEMG at a specific time point. SD is a statistical measure of dispersion, indicating the variability or spread of a dataset. In the muscle mechanical signals, SD can describe the variability in the amplitude of signals, directly reflecting the strength of the tremor. The magnitude of SD can be used to assess the level of muscle

$$\text{fatigue. Its calculation formula is } SD = \sqrt{\frac{1}{k-1} \sum_{i=1}^k (x_i - \bar{x})^2},$$

where x_i represents the output of the FMG sensor for a selected period, and \bar{x} represents the mean value of this data segment. As the fatigue stage approaches (as depicted in the seventh cycle of the figure), the RMS

value of the sEMG signal significantly decreases, while the SD value of the FMG signal noticeably increases. Hence, these two metrics can be used as characteristics of electrical and mechanical signals, respectively, to reflect the level of muscle fatigue. After performing STFT and FFT on the sEMG and FMG signals separately, the results reveal that (Figures S12 and S13), as muscle fatigue increases, the frequency distribution of the sEMG signal remains relatively unchanged. In contrast, the proportion of the FMG signal within the 10–20 Hz frequency range (the tremor frequency range) significantly increases.

Data analysis shows that for active muscle contractions in healthy individuals, the amplitudes of sEMG and FMG signals are correlated: stronger muscle force leads to higher amplitudes in both. However, their frequencies are not correlated. The frequency of sEMG reflects muscle fiber recruitment and activation levels, indicating muscle strength and fatigue, while FMG frequency reflects changes in mechanical signals, such as the frequency of continuous movements and muscle tremors during contraction. Assessing muscle state is complex because sEMG signal amplitude and frequency are influenced by muscle strength, fatigue, and whether the muscle contraction is active or passive. Therefore, sEMG alone cannot accurately evaluate muscle strength and fatigue. Similarly, FMG signal amplitude is influenced by the extent and speed of muscle deformation, and its frequency by the frequency of continuous movements and muscle tremors during fatigue, making FMG alone insufficient for accurate assessment of muscle state during active contraction. When analyzing the temporally synchronized signals of both types together, it is possible to accurately evaluate the muscle state during active contraction based on their combined characteristics from the temporally synchronized sEMG and FMG signals monitored by PCSP. For instance, muscle strength during active contraction can be inferred from the simultaneous increase or decrease in both sEMG and FMG amplitudes. Muscle fatigue can be accurately assessed by a decrease in sEMG amplitude and an increase in FMG tremor frequency.

2.5 | Application in the evaluation of muscle dysfunction

Parkinson's disease (PD) is a neurodegenerative condition largely marked by motor abnormalities, including bradykinesia and muscle rigidity. These motor symptoms manifest through the abnormal characteristics observed in muscle-related behaviors. Bradykinesia is one of the core features of PD, referring to the slowness of movement that is characterized by a reduction in amplitude or speed when a motion is continuously repeated. During

clinical practice, a patient's bradykinesia is often evaluated through a subjective assessment and scoring. Here, we specifically investigated the characteristics of muscle contraction in Parkinson's patients exhibiting symptoms of bradykinesia using the developed PCSP. A clinical gold-standard scale motion test was conducted on typical PD patients to evaluate the condition, which involves rapid foot stomping and toe-tapping. Two PD patients with typical bradykinesia symptoms, aged between 50 and 60, were tested. Their sEMG and FMG signals exhibited similar characteristics.

Figure 5A illustrates a schematic based on the PCSP test for the foot stomping action. The primary muscles involved in this action are the gastrocnemius and the tibialis anterior, located in the lower leg, which act as the agonist and antagonist muscles, respectively. Two PCSP units are attached to the skin overlying tibialis anterior and gastrocnemius muscles, respectively, after which the patient is asked to perform the foot stomping action as quickly as possible for a duration of 15 s. Figure 5B,C depicts the sEMG output of a healthy individual and a PD patient while performing the fast foot stomping movement. Additionally, the figures display the time-frequency graphs obtained after applying the STFT processing. Figure 5D,E presents the corresponding FMG output and the time-frequency graphs after STFT processing, with the left side showing the gastrocnemius muscle and the right side showing the tibialis anterior.

Analysis of the original sEMG signal waveforms from both healthy individual and PD patient shows that the sEMG amplitude of the agonist muscle is greater than that of the antagonist muscle. Simultaneously, the 15-s power spectral density depicted in Figure S14 reveals that the sEMG output of the gastrocnemius muscle demonstrates a greater peak density at high frequencies in comparison to that of tibialis anterior. In addition, the sEMG signals of healthy individual have higher power at high frequencies compared to those of patients with PD. These amplitude-frequency characteristics are also observed in the action of rapid toe tapping (with the tibialis anterior acting as the agonist muscle and the gastrocnemius as the antagonist muscle), as shown in Figure S15. The FMG signal amplitudes show no significant difference between the two muscles, but the direction of the peaks is exactly opposite. This occurs because during the process of foot dorsiflexion, the gastrocnemius muscle is in a state of contraction, while the tibialis anterior muscle is in a condition of extension. Consequently, the muscle fibers of these two muscles undergo deformation in different directions, resulting in opposite peaks in the output waveform of the FMG sensor.

As rapid movements continue, the amplitude of the sEMG signal of the gastrocnemius muscle in PD patient decreases quickly, and the output of the FMG sensors for

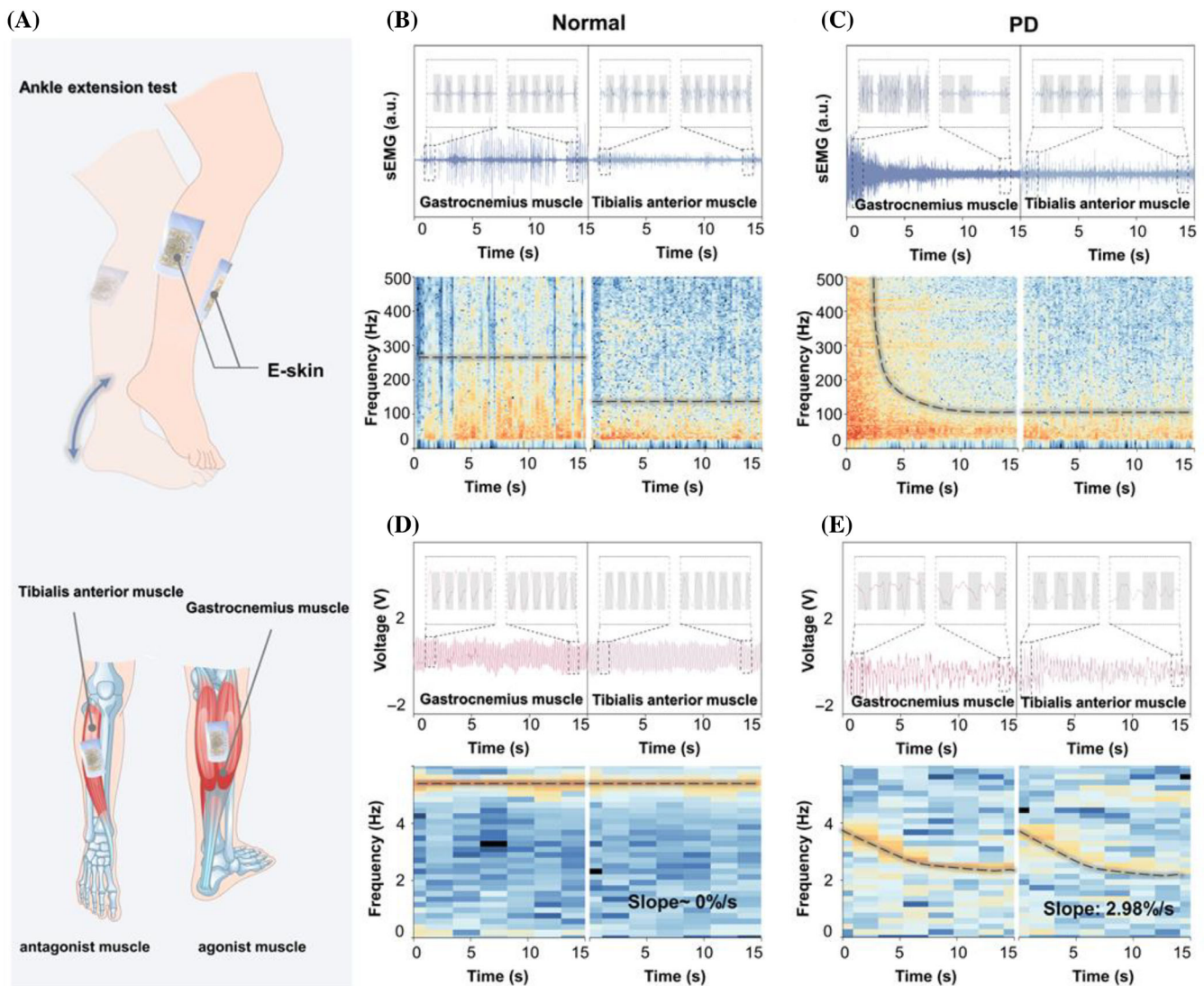


FIGURE 5 Muscle state testing of PD patients with motor disorders such as bradykinesia using PCSP during scale movement tasks. (A) Illustration of rapid foot stomping action and schematic diagram of PCSP placement on the antagonistic muscle pair of gastrocnemius and tibialis anterior. (B) The sEMG electrode outputs of the two muscles (top) and the corresponding time-frequency graphs after STFT (bottom) during the rapid foot stomping process in normal individuals. (C) The sEMG electrode outputs of the two muscles (top) and the corresponding time-frequency graphs after STFT (bottom) during the rapid foot stomping process in PD patients. (D) The FMG sensor outputs of the two muscles (top) and the corresponding time-frequency graphs after STFT (bottom) during the rapid foot stomping process in normal individuals. (E) The FMG sensor outputs of the two muscles (top) and the corresponding time-frequency graphs after STFT (bottom) during the rapid foot stomping process in PD patients.

both muscles also decline over time, whereas in healthy individual, it remains stable throughout the 15-s action. The reason for this is that patients with PD experience movement bradykinesia and rapid fatigue due to their continuous and fast movements. These are manifested as a decrease in the activation level of muscle fibers and a reduction in the amplitude and frequency of muscle deformation. This corresponds to a decrease in the frequency of sEMG signals and a reduction in the amplitude frequency of FMG sensor outputs. The time-frequency graphs of both sensors exhibit these

characteristics, with no noticeable decline detected in health individuals.

In the start of the sEMG time-frequency graph of PD patients, there is an explosive increase in the frequency of the electromyographic signal, which is a typical characteristic of Parkinsonian bradykinesia caused by a lack of dopamine. Patients, in order to overcome the difficulty of starting movements, often need to activate more neuromuscular fibers, manifesting as a high frequency at the initial state. The time-frequency graph of FMG includes a quantitative index $S = \frac{1}{t} \frac{f_e - f_i}{f_i}$ that displays the time

domain characteristics of muscle contraction deformation, where f_e represents the frequency at the end of the selected time period, f_i represents the frequency at the beginning of the selected time period, and t represents the duration of the selected time. By analyzing the FMG time-frequency graph, it is evident that the frequency of muscle mechanical deformation is generally greater in healthy individual compared to PD patient. Concurrently, the S value for healthy individual is about 0, whereas for patient with PD, it is 2.98% per second. This value can be utilized to measure the rate at which muscles become tired and to evaluate the extent of bradykinesia in patients with PD. During the quick toe-tapping movement depicted in Figure S15, individuals with PD demonstrate similar characteristics in both amplitude and frequency in both sEMG and FMG signals.

For PD patients, their bradykinesia, characterized by difficulty in initiating movement and a decrease in continuous movement frequency, can be reflected by two distinct features in sEMG and FMG signals. The abrupt increase and decrease in sEMG signals and the sustained decline in FMG signals can differentiate PD patients from healthy individuals. To further explore the potential application of PCSP in distinguishing abnormal muscle states, we tested the differences in both sEMG and FMG synchronous signals during voluntary and involuntary contractions. As shown in Figure S16, compared to active muscle contractions, the involuntary muscle contractions lack the high-frequency components of the EMG signal. This is due to the absence of muscle fibers recruitment during passive contractions, resulting in a decrease in muscle fiber discharge. For FMG, although there is still muscle deformation during passive contractions, the tremor signals during muscle deformation decrease or almost disappear. Therefore, although the FMG signal can indicate muscle deformation, combining it with the sEMG signal can provide a more accurate assessment of the contraction state of the muscle.

3 | CONCLUSION

In daily activities, the varied behaviors of muscles contain multiple types of information, with sEMG signals indicating the level of muscle fiber activation, and FMG signals representing the amplitude and frequency of muscle deformation and tremor during muscle contractions. To monitor the complementary electrical and mechanical signals during muscle activities and to gain a more comprehensive understanding of muscle status, this work has presented a novel patterned electrical-mechanical coupled sensing patch (PCSP). The PCSP is designed to

be affixed to the skin overlying the muscles for the multimodal evaluation of different muscle regions. Incorporating stretchable serpentine sEMG electrodes and a fingerprint-like piezoelectric FMG sensor, PCSP was integrated through two ultra-thin layers of PDMS. Theoretical calculations and experiment testing have demonstrated that the PCSP maintains excellent stretchability, preserving its functionality after 15 000 cycles of 30% repetitive strain. A thermo-responsive adhesive hydrogel is employed here to reduce the resistance between the patterned sEMG dry electrode and the skin and to ensure that the FMG sensor maintains the required preload force during muscle deformation. The sEMG signal achieves an SNR of 33.07 dB during continuous muscle monitoring, while the FMG sensor demonstrates dependable and uniform performance, attributed to the adhesive layer. The combined use of sEMG electrodes and FMG sensor enables the capture of both the electrical and mechanical information of muscle contractions synchronously, providing a comprehensive analysis of muscle strength and fatigue through complementary time and frequency characteristics. PD patients with typical bradykinesia symptoms showed unique time-frequency signal features compared to healthy individuals in ankle extension tests, with sharp rises and falls in sEMG signal frequency and distinct low-frequency traits observed by FMG sensor, showing the diagnostic assessment potential of PCSP for muscular dysfunction. The effectiveness and convenience of PCSP in multimodal muscle evaluations, including muscle strength, fatigue, and dysfunction, make it a promising tool for application in exercise training and rehabilitation monitoring.

Existing related studies mostly utilize various sensing devices, such as sEMG and FMG sensors, to achieve motion detection and gesture recognition. Although AI-based algorithm models offer high recognition accuracy and fast processing times, most of these studies directly integrate rigid sensing unit arrays into armbands, leading to certain limitations in the size, portability, and comfort of the devices. By comparing the performance metrics across various aspects, the proposed PCSP offers advantages in terms of thinness, stretchability, signal quality, and comfort (Table S1). However, there are still some issues to be solved. For instance, the current patch area is large, which makes it susceptible to interference from multiple muscles. Future improvements will focus on reducing the electrode area and increasing electrode density to achieve high-precision monitoring of individual muscle states. Additionally, future developments will incorporate flexible electronics to enhance system integration, creating a unified module for signal acquisition, information processing, and transmission. In addition to

clinical applications, using the characteristics of forearm and hand muscle motion signals extracted by PCSP, combined with emerging artificial intelligence technologies, it is also expected to play a role in man-machine interaction fields such as gesture recognition and prosthetic control.

4 | EXPERIMENTAL SECTION

4.1 | Fabrication of the serpentine structured sEMG electrode

The electrodes are prepared by sputtering a metal layer on the PI film, followed by patterned cutting with a film cutter. A 50- μm thick PI film is selected and cut to a size of 10 cm in length and width, followed by ultrasonic cleaning and drying as a pretreatment. On the pretreated PI film, a layer of chromium is first sputtered using a magnetron sputtering (Discovery635, Denton) method, with a sputtering power of 100 W for 5 min, achieving a sputter thickness of approximately 20 nm. After sputtering the chromium layer, a gold layer is sputtered with a power of 100 W for 30 min, achieving a thickness of approximately 100 nm. The film cutter (Cricut Maker 3) is used for patterned cutting of the film: The prepared electrode film is placed flat on a sticky pad to ensure no bubbles form, the appropriate cutting parameters are set, and the cutting process is initiated. Excess parts are removed, and a preprepared PDMS transfer layer is affixed to the cut electrode surface. After ensuring proper adhesion with pressure, the assembly is heated on a constant temperature platform at 60 degrees Celsius for 30 min. The PDMS layer is then removed, and the electrode layer is slowly peeled off from the PDMS. The removed electrode layer is placed into deionized water for ultrasonic cleaning for 15 min, followed by drying, to complete the preparation of patterned sEMG electrodes.

4.2 | Fabrication of the fingerprint-like FMG sensors

The fingerprint-like FMG sensors are obtained by cutting commercial silver-plated PVDF film. Cut the 52- μm thick silver-plated PVDF into dimensions of 5 centimeters in length and 5 centimeters in width, then adhere a layer of 8- μm thick PTFE onto the surface of the PVDF film. Lastly, a 5- μm thick layer of PI single-sided adhesive tape is applied to the outer layer of the PTFE. This layer of adhesive tape serves the purpose of preventing a short circuit between the top and bottom surfaces during the cutting process of the silver-plated PVDF. Place

the pretreated PVDF film on the pad of the mechanical stamping press, and use the patterned cutting tool prepared in the first step to perform the cutting. After cutting, remove the PVDF film and eliminate the excess parts. Then, use a cotton swab dipped in ethanol to wipe the edges of the patterned structure. This step is designed to prevent a short circuit between the upper and lower surfaces caused by the residual silver layer during the stamping cutting process. Finally, remove the single-sided PI tape from the surface.

4.3 | Fabrication of the thermally enhanced adhesive hydrogel

Rinse the pre-3D printed polylactic acid mold and two flat glass plates with deionized water in an ultrasonic bath for a duration of 10 min, followed by drying. Measure out 9 mL of deionized water and pour it into a beaker. Next, add approximately 4–5 g of CaCl_2 to the deionized water. Following dissolution, incorporate 1 g of b-PEI (with a molecular weight of 600) and introduce a magnetic stir bar to accelerate the process of dissolve. Lastly, incorporate 2 g of PVA (type 1799) into the mixture. Then, subject the mixture to a water bath at a temperature of 95°C and maintain magnetic stirring for a duration of 2 h. After forming a uniform solution, pour the uniform solution into the mold assembly comprising the polylactic acid mold and glass plates, secure it with clamps, and freeze for 12 h in a freezer at -20°C . Then, thaw for 6 h at 25°C to complete the preparation.

4.4 | Characterization and measurements

A digital tensile force gauge (Mark-10) is used to perform stretch testing on PCSP. An oscilloscope (LeCroy, HDO6104) was used for measuring the open-circuit voltage of the FMG sensor and store the data during the stretch test. An electrometer (Keithley 6517) was used for measuring the current and charge of FMG sensor during the stretch test. The wearable experimental test of this study was approved by the Medical Experiment Ethics Committee of Beijing Institute of Nanoenergy and Nanosystems (Approval No. 2023015LZ).

4.5 | Calculation of sEMG SNR

After acquiring the sEMG signal via Bluetooth of signal acquisition circuit board, a band-pass filter ranging from 15 to 500 Hz is applied. The Fast Fourier Transform

(FFT) is utilized to identify the predominant noise, which is determined to be 50 Hz power line interference. Subsequently, the power spectral density (PSD) of the noise frequency range and the effective signal, are calculated using the Welch method. This process results in the PSD of the noise and the PSD of the EMG signal. Finally, the signal-to-noise ratio (SNR) is calculated using the following formula:

$$\text{SNR (dB)} = 10 \cdot \log_{10} \left(\frac{P_{\text{noise}}}{P_{\text{signal}}} \right).$$

ACKNOWLEDGMENTS

This study was supported by the National Key Research and Development Program of China (2022YFE0111700), the National Natural Science Foundation of China (T2125003, 82202075), Beijing Natural Science Foundation (L212010), the National Postdoctoral Program for Innovative Talents (BX20220380), China Postdoctoral Science Foundation (2022M710389), and the Fundamental Research Funds for the Central Universities.

CONFLICT OF INTEREST STATEMENT

The authors declare no conflicts of interest.

ORCID

Zhou Li  <https://orcid.org/0000-0002-9952-7296>

REFERENCES

- Enoka RM, Duchateau J. Muscle fatigue: what, why and how it influences muscle function. *J Physiol*. 2008;586(1):11-23.
- Kuriki HU, Mello EM, De Azevedo FM, Takahashi LSO, Alves N, de Faria Negrão Filho R. The relationship between electromyography and muscle force. In: *EMG Methods for Evaluating Muscle and Nerve Function*. Rijeka: INTECH Open Access Publisher, 2012. 33-54.
- Cifrek M, Medved V, Tonković S, Ostojić S. Surface EMG based muscle fatigue evaluation in biomechanics. *Clin Biomech*. 2009;24(4):327-340.
- Orizio C. Muscle sound: bases for the introduction of a mechanomyographic signal in muscle studies. *Crit Rev Biomed Eng*. 1993;21(3):201-243.
- Krueger E, Scheeren EM, Nogueira-Neto GN, Button VLSN, Nohama P. Advances and perspectives of mechanomyography. *Rev Bras Eng Bioméd*. 2014;30(4):384-401.
- Esposito D, Andreozzi E, Fratini A, et al. A piezoresistive sensor to measure muscle contraction and mechanomyography. *Sensors*. 2018;18(8):2553.
- Tan P, Han X, Zou Y, et al. Self-powered gesture recognition wristband enabled by machine learning for full keyboard and multicommand input. *Adv Mater*. 2022;34(21):2200793.
- Zou Y, Tan P, Shi B, et al. A bionic stretchable nanogenerator for underwater sensing and energy harvesting. *Nat Commun*. 2019;10(1):2695.
- Al-Mulla MR, Sepulveda F, Colley M. A review of non-invasive techniques to detect and predict localised muscle fatigue. *Sensors*. 2011;11(4):3545-3594.
- Alvarez JT, Gerez LF, Araromi OA, et al. Towards soft wearable strain sensors for muscle activity monitoring. *IEEE Trans Neural Syst Rehabil Eng*. 2022;30:2198-2206.
- Gong Q, Jiang X, Liu Y, Yu M, Hu Y. A flexible wireless sEMG system for wearable muscle strength and fatigue monitoring in real time. *Adv Electron Mater*. 2023;9(9):2200916.
- Chapman J, Dwivedi A, Liarakapis M. A wearable, open-source, lightweight forcemyography armband: on intuitive, robust muscle-machine interfaces. *IEEE*; 2021:4138-4143.
- Ergeneci M, Gokcesu K, Ertan E, Kosmas P. An embedded, eight channel, noise canceling, wireless, wearable sEMG data acquisition system with adaptive muscle contraction detection. *IEEE Trans Biomed Circ Syst*. 2017;12(1):68-79.
- Islam MA, Sundaraj K, Ahmad RB, Ahamed NU. Mechanomyogram for muscle function assessment: a review. *PLoS One*. 2013;8(3):e58902.
- Knezevic OM, Mirkov DM, Kadija M, Milovanovic D, Jaric S. Evaluation of isokinetic and isometric strength measures for monitoring muscle function recovery after anterior cruciate ligament reconstruction. *J Strength Cond Res*. 2014;28(6):1722-1731.
- Bosco C, Colli R, Bonomi R, von Duvillard SP, Viru A. Monitoring strength training: neuromuscular and hormonal profile. *Med Sci Sports Exerc*. 2000;32(1):202-208.
- Lerario A, Bonfiglio S, Sormani M, et al. Quantitative muscle strength assessment in duchenne muscular dystrophy: longitudinal study and correlation with functional measures. *BMC Neurol*. 2012;12(1):1-8.
- Wang C, Qu X, Zheng Q, et al. Stretchable, self-healing, and skin-mounted active sensor for multipoint muscle function assessment. *ACS Nano*. 2021;15(6):10130-10140.
- Phinyomark A, Campbell E, Scheme E. Surface electromyography (EMG) signal processing, classification, and practical considerations. *Biomedical Signal Processing: Advances in Theory, Algorithms and Applications*. Singapore: Springer; 2020:3-29.
- Sung JH, Baek S-H, Park J-W. Surface electromyography-driven parameters for representing muscle mass and strength. *Sensors*. 2023;23(12):5490.
- Zhang S, Guo S, Gao B, et al. Muscle strength assessment system using sEMG-based force prediction method for wrist joint. *J Med Biol Eng*. 2016;36(1):121-131.
- Clancy EA, Morin EL, Hajian G, et al. Surface electromyogram (sEMG) amplitude estimation: Best practices. *J Electromyogr Kinesiol*. 2023;72:102807.
- Athavale Y, Krishnan S. Biosignal monitoring using wearables: observations and opportunities. *Biomed Signal Process Control*. 2017;38:22-33.
- Xiao ZG, Menon C. A review of force myography research and development. *Sensors*. 2019;19(20):4557.
- Zheng Z, Wu Z, Zhao R, Ni Y, Jing X, Gao S. A review of EMG-, FMG-, and EIT-based biosensors and relevant human-machine interactivities and biomedical applications. *Biosensors*. 2022;12(7):516.
- Boyas S, Guével A. Neuromuscular fatigue in healthy muscle: underlying factors and adaptation mechanisms. *Ann Phys Rehabil Med*. 2011;54(2):88-108.

27. Wan J, Qin Z, Wang P, Sun Y, Liu X. Muscle fatigue: general understanding and treatment. *Exp Mol Med*. 2017;49(10):e384.
28. Garcia-Retortillo S, Romero-Gómez C, Ivanov PC. Network of muscle fibers activation facilitates inter-muscular coordination, adapts to fatigue and reflects muscle function. *Commun Biol*. 2023;6(1):891.
29. Ferigo D, Merhi L-K, Pousett B, Xiao ZG, Menon C. A case study of a force-myography controlled bionic hand mitigating limb position effect. *J Bionic Eng*. 2017;14(4):692-705.
30. Truong H, Zhang S, Muncuk U, et al. Capband: battery-free successive capacitance sensing wristband for hand gesture recognition; 2018: 54-67.
31. Choi Y, Lee S, Sung M, Park J, Kim S, Choi Y. Development of EMG-FMG based prosthesis with PVDF-film vibrational feedback control. *IEEE Sens J*. 2021;21(20):23597-23607.
32. Wu YT, Gomes MK, da Silva WH, Lazari PM, Fujiwara E. Integrated optical fiber force myography sensor as pervasive predictor of hand postures. *Biomed Eng Comput Biol*. 2020;11:1179597220912825.
33. Jiang S, Gao Q, Liu H, Shull PB. A novel, co-located EMG-FMG-sensing wearable armband for hand gesture recognition. *Sens Actuators, A*. 2020;301:111738.
34. Shahandashti PF, Pourkheyrollah H, Jahanshahi A, Ghafoorifard H. Highly conformable stretchable dry electrodes based on inexpensive flex substrate for long-term biopotential (EMG/ECG) monitoring. *Sens Actuators, A*. 2019;295:678-686.
35. Jung P-G, Lim G, Kim S, Kong K. A wearable gesture recognition device for detecting muscular activities based on air-pressure sensors. *IEEE Trans Industr Inform*. 2015;11(2):485-494.
36. Cai P, Wan C, Pan L, et al. Locally coupled electromechanical interfaces based on cytoadhesion-inspired hybrids to identify muscular excitation-contraction signatures. *Nat Commun*. 2020;11(1):2183.
37. Herrera-Luna I, Rechy-Ramirez EJ, Rios-Figueroa HV, Marin-Hernandez A. Sensor fusion used in applications for hand rehabilitation: a systematic review. *IEEE Sens J*. 2019;19(10):3581-3592.
38. Tang W, Li C, Wang T, et al. Deep-learning model coupling wearable bioelectric and mechanical sensors for refined muscle strength assessment. *Research*. 2024;7:0366.
39. Nordez A, Gallot T, Catheline S, Guével A, Cornu C, Hug F. Electromechanical delay revisited using very high frame rate ultrasound. *J Appl Physiol*. 2009;106(6):1970-1975.
40. Gurev V, Constantino J, Rice J, Trayanova NA. Distribution of electromechanical delay in the heart: insights from a three-dimensional electromechanical model. *Biophys J*. 2010;99(3):745-754.
41. Ahmadizadeh C, Merhi LK, Pousett B, Sangha S, Menon C. Toward intuitive prosthetic control: solving common issues using force myography, surface electromyography, and pattern recognition in a pilot case study. *IEEE Robotics & Automation Magazine*; 2017, 24(4): 102-111.
42. Chen P, Li Z, Togo S, Yokoi H, Jiang Y. A layered sEMG-FMG hybrid sensor for hand motion recognition from forearm muscle activities. *IEEE Transactions on Human-Machine Systems*; 2023, 53(5): 935-944.
43. Islam MRU, Waris A, Kamavuako EN, Bai S. A comparative study of motion detection with FMG and sEMG methods for assistive applications. *J Rehabil Assist Technol Eng*. 2020;7: 2055668320938588.
44. Chen Z, Wang H, Chen H, Wei T. Continuous motion finger joint angle estimation utilizing hybrid sEMG-FMG modality driven transformer-based deep learning model. *Biomed Signal Process Control*. 2023;85:105030.
45. Zou Y, Gai Y, Tan P, et al. Stretchable graded multichannel self-powered respiratory sensor inspired by shark gill. *Fundam Res*. 2022;2(4):619-628.
46. Fu R, Tu L, Zhou Y, et al. A tough and self-powered hydrogel for artificial skin. *Chem Mater*. 2019;31(23):9850-9860.
47. Liu Y, Wang C, Xue J, et al. Body temperature enhanced adhesive, antibacterial, and recyclable ionic hydrogel for epidermal electrophysiological monitoring. *Adv Healthc Mater*. 2022; 11(15):2200653.
48. Liu Y, Wang C, Liu Z, et al. Self-encapsulated ionic fibers based on stress-induced adaptive phase transition for non-contact depth-of-field camouflage sensing. *Nat Commun*. 2024;15(1):663.
49. Wang C, Liu Y, Qu X, et al. Ultra-stretchable and fast self-healing ionic hydrogel in cryogenic environments for artificial nerve fiber. *Adv Mater*. 2022;34(16):2105416.
50. Nam S, Mooney D. Polymeric tissue adhesives. *Chem Rev*. 2021;121(18):11336-11384.
51. Yuk H, Varela CE, Nabzdyk CS, et al. Dry double-sided tape for adhesion of wet tissues and devices. *Nature*. 2019;575(7781): 169-174.

SUPPORTING INFORMATION

Additional supporting information can be found online in the Supporting Information section at the end of this article.

How to cite this article: Xue J, Zou Y, Wan Z, et al. A patterned mechanical–electrical coupled sensing patch for multimodal muscle function evaluation. *InfoMat*. 2024;e12631. doi:10.1002/inf2.12631